Mesoscopic Metal Nanoparticles Doubly Functionalized with Natural and Engineered Lipidic Dispersants for Therapeutics

Tatsuya Murakami,[†,*] Hirotaka Nakatsuji,[‡] Nobuhiro Morone,[†] John E. Heuser,[†] Fumiyoshi Ishidate,[†] Mitsuru Hashida,[†,§] and Hiroshi Imahori[†,‡,*]

[†]Institute for Integrated Cell-Material Sciences (WPI-iCeMS), Kyoto University, Sakyo-ku, Kyoto 606-8501, Japan, [‡]Department of Molecular Engineering, Graduate School of Engineering, Kyoto University, Nishikyo-ku, Kyoto 615-8510, Japan, and [§]Department of Drug Delivery Research, Graduate School of Pharmaceutical Sciences, Kyoto University, Sakyo-ku, Kyoto 606-8501, Japan

ABSTRACT Surface engineering of mesoscopic metal nanoparticles to increase biocompatibility and cell interaction is important for improvement of their therapeutic properties. Here, we describe a strategy to stabilize mesoscopic metal nanoparticles and to enhance their cell interaction by stepwise addition of (*Z*)-9-octadecenoate (oleate) and a cell-penetrating peptide-fused high-density lipoprotein (cpHDL). Oleate replaces a cytotoxic dispersant on the surface of gold nanorods (AuNRs), which enables subsequent cpHDL binding without causing aggregation. Notably, these two lipidic dispersants are probably intercalated on the surface. This procedure was also used to stabilize 20 nm spherical gold nanoparticles and 40 nm aggregates of 10 nm magnetite nanoparticles. cpHDL-bound AuNRs were internalized greater than 80 times more efficiently than poly(ethylene glycol)-conjugated AuNRs and were able to elicit cancer cell photoablation.

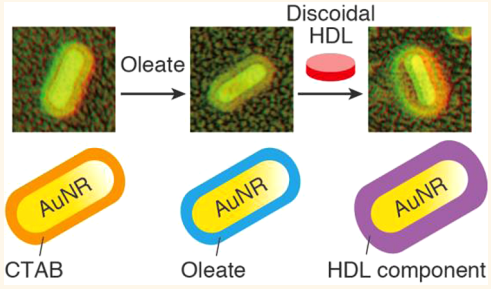

KEYWORDS: gold nanorod · magnetite nanoparticle · oleate · high-density lipoprotein · internalization · photothermal effect

Controlling the surface chemistry of mesoscopic nanoparticles (5−100 nm) is particularly important when attempting to develop stimulus-responsive metal nanoparticles, which have recently attracted attention due to their potential utility as localized and noninvasive ablators of tumors.[1,2] The gold nanorod (AuNR) is a particularly promising type of metal nanoparticle. AuNRs are a highly efficient photothermal conversion material[3−5] that can be used for tumor ablation. AuNRs also emit strong two-photon luminescence that is currently being studied for deep tissue imaging.[6−9] Since "raw" AuNRs are extremely cytotoxic, due largely to cetyltrimethylammonium bromide (CTAB) on their surface,[10] poly(ethylene glycol) (PEG), a biocompatible dispersant, is widely used in the development of AuNRs as therapeutic agents.[11−13] Theoretically, biocompatible and cell-interactive AuNRs could be used to ablate tumors through localized heating, as well as to deliver oligonucleotides intracellularly.[14−17] However, PEGylation does not enhance the cell interactivity of nanoparticles, and PEGylated AuNRs are repelled from a number of cell types.[18,19] In addition, conjugation of cell surface receptor ligands to PEGylated liposomes prepared in a standard way did not enhance their cell uptake,[20] perhaps due to the globular mushroom-like structures of the long PEG molecules hindering accessibility of the ligand on the liposome surface.

Our basic strategy for preparation of biocompatible and cell-interactive mesoscopic metal nanoparticles is to utilize natural molecules that interact with tissues and cells. (*Z*)-9-Octadecenoate (oleate)[21] and high-density lipoprotein (HDL)[22] (a mediator of reverse cholesterol transport) are examples of these molecules. In this study, we sought to enhance the interaction of mesoscopic metal nanoparticles with cells by genetically fusing a cell-penetrating peptide (TAT) to

* Address correspondence to murakami@icems.kyoto-u.ac.jp, imahori@scl.kyoto-u.ac.jp.

Received for review May 6, 2014 and accepted June 14, 2014.

Published online June 14, 2014
10.1021/nn5024818

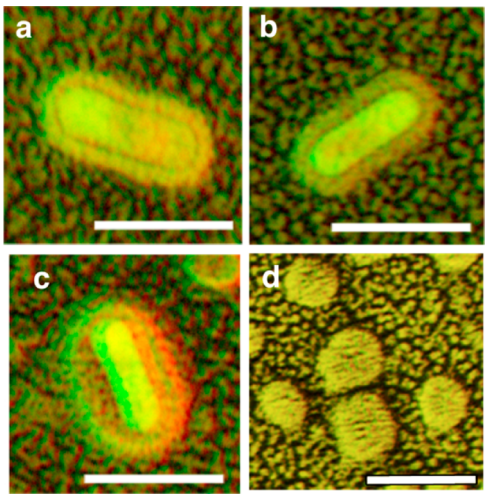

Figure 1. Mica flake transmission electron microscopy (TEM) images. (a) CTAB-AuNRs; (b) oleate-AuNRs; (c) cpHDL-AuNRs (R = 250); (d) cpHDL (R = 250). cpHDL (R = 250) had a discoidal structure with an average diameter of *ca.* 20 nm, suggesting that it has a discoidal phospholipid bilayer, similarly to native HDL. Scale bar, 50 nm.

the HDL.[23] The TAT peptide has high homology with human protein (85−95%)[24] and has been examined in more than 25 clinical trials for the delivery of therapeutic molecules.[25]

RESULTS AND DISCUSSION

HDLs were prepared by mixing 1-palmitoyl-2-oleoyl-*sn*-glycero-3-phosphocholine (POPC) and apoA-I or its mutant fused with TAT peptide at a lipid/protein molar ratio of 100 (denoted as R = 100) or 250 (R = 250).[26] The mean hydrodynamic diameter of cell-penetrating peptide-fused high-density lipoprotein (cpHDL) (R = 250) on a volume basis was determined to be 36 nm by dynamic light scattering analysis, which was larger than that of cpHDL (R = 100) (14 nm) (Supporting Information Figure S1). The diameter of cpHDL (R = 250) was 20 ± 9.1 nm under vacuum in mica flake transmission electron microscopy imaging (Figure 1d) (see Methods section).

CTAB-capped AuNRs (CTAB-AuNRs) had a length of 54 ± 10 nm and an aspect ratio of 3.3 ± 0.3 (Figure 1a). Upon treatment of CTAB-AuNRs with oleate, the colloidal stability of the AuNRs (oleate-AuNRs) in phosphate buffer saline (PBS) improved relative to CTAB-AuNRs, and the longitudinal plasmon peak of CTAB-AuNRs was blue-shifted (Figure S2). Such a blue shift could in part be due to shortening of the AuNRs during oleate treatment (42 ± 5.2 nm in length and aspect ratio of 2.7 ± 0.5) (Figure 1b).[17] Simultaneously, we made the first observation of thin organic layers (*ca.* 3.8 and 4.0 nm) for CTAB-AuNRs and oleate-AuNRs (Figure 1a,b and Figure S3a,b) using our TEM technique. The zeta-potential of the CTAB-AuNRs markedly decreased from 25 ± 2.1 to −39 ± 4.7 mV. In X-ray photoelectron spectroscopy (XPS) spectra, peaks

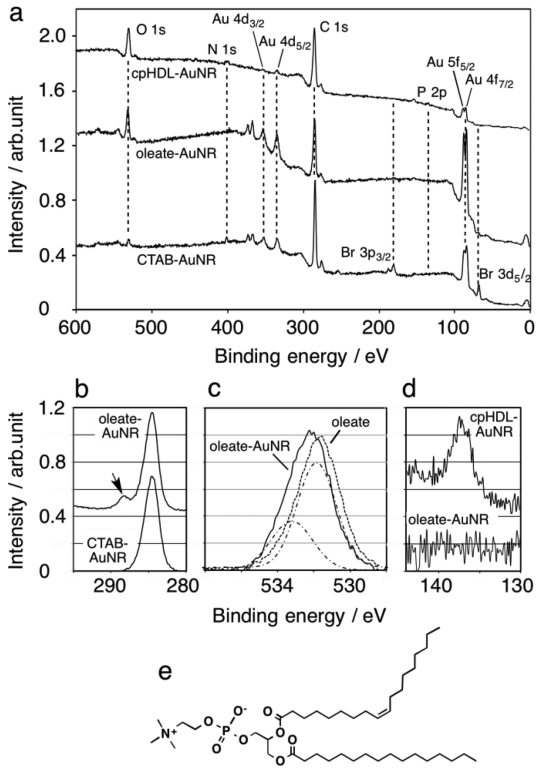

Figure 2. X-ray photoelectron spectroscopy analysis. Spectra of CTAB-, oleate-, and cpHDL-AuNRs (R = 250) (a) and magnified spectra for (b) C 1s, (c) O 1s, and (d) P 2p. In (c), the original spectrum of oleate-AuNRs (—) was fitted by two Gaussian functions (— · —) using OriginPro 8.6. The spectrum of neat sodium oleate (---) is shown for comparison. (e) Chemical structure of POPC.

arising from CTAB largely disappeared after oleate treatment (Figure 2a), and peaks assignable to carboxylate groups were detected at 288.4 and 532.2 eV (Figure 2b,c). These observations unambiguously demonstrate that CTAB on the CTAB-AuNRs is almost entirely replaced by oleate. The O 1s peak was deconvoluted into two peaks (Figure 2c), suggesting the presence of an oleate bilayer on the AuNR surface, as observed for magnetite nanoparticles.[27−29] In agreement with the XPS data, the ^{1}H NMR resonance for the γ-CH_3 protons of CTAB disappeared and IR signals assignable to the carboxylate group of oleate were detected after oleate treatment of CTAB-AuNRs (Figures S4 and S5).

Oleate-AuNRs were then mixed with cpHDL (R = 250) at 50 °C in PBS for 1 h at a cpHDL/AuNR weight ratio of 0.4 (*vide infra*), centrifuged to discard the supernatant, and redispersed in PBS. After mixing, the thickness of the organic layer increased significantly (Figure 1c). The average thickness was *ca.* 7.0 nm (Figure S3d). The longitudinal length and aspect ratio (42 ± 3.1 nm and 2.7 ± 0.4) of the cpHDL (R = 250)-treated oleate-AuNRs (cpHDL-AuNRs (R = 250)) were almost the same as those of oleate-AuNRs (Figure 1b). There was negligible broadening of the plasmon peak of oleate-AuNRs after treatment with cpHDL (R = 250) (Figure S2b).

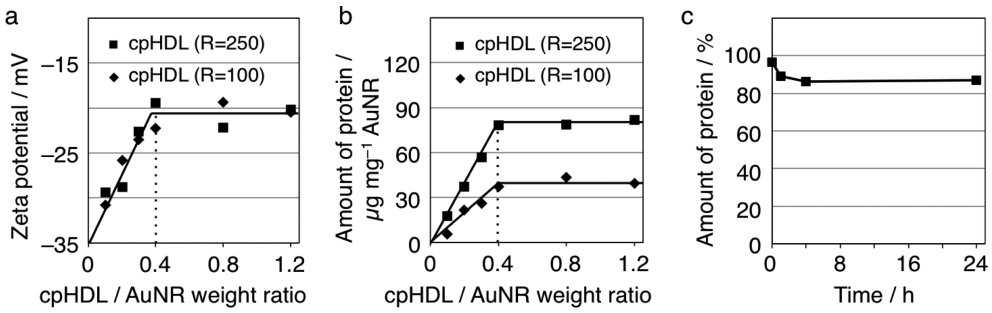

Figure 3. Quantitative analyses of cpHDL binding to oleate-AuNRs and cpHDL release from cpHDL-AuNRs (R = 250). (a) Zeta-potential after addition of cpHDL to oleate-AuNRs at various cpHDL/AuNR weight ratios. (b) Amount of cpHDL adsorbed to oleate-AuNRs at various cpHDL/AuNR weight ratios. (c) Time-dependent change in the amount of cpHDL in cpHDL-AuNRs (R = 250). The amount of cpHDL was determined based on fluorescence intensity from the protein moiety (see Methods). cpHDL-AuNRs (R = 250) were dispersed in PBS, incubated at 37 °C, and centrifuged at the indicated times. The pellets were subjected to SDS-PAGE and densitometry. Data were standardized to the fluorescence intensity before dispersion.

cpHDL-AuNRs (R = 250) showed excellent colloidal stability after 1 week of incubation in PBS at 37 °C, comparable to that of PEG-conjugated AuNRs (PEG-AuNRs) (Figure S6a,b). The stability only changed slightly in the presence of serum (Figure S6c). Direct treatment of CTAB-AuNRs with cpHDL (R = 250) resulted in slight aggregation of AuNRs just after preparation (Figure S7a), clearly showing the advantage of oleate pretreatment on stabilization using cpHDL. The AuNRs obtained by direct cpHDL treatment were also still highly cytotoxic (Figure S7b).

The zeta-potential of cpHDL-AuNRs (R = 250) was -21 ± 1.5 mV, which was higher than that of -39 ± 4.7 mV for oleate-AuNRs, but still negative. Simultaneously, the IR signal for the carboxylate group of oleate was retained after cpHDL (R = 250) treatment of oleate-AuNRs (Figure S5), and the N 1s peak (Figure 2a) and P 2p peak (Figure 2d) derived from POPC (Figure 2e) appeared in the XPS spectrum of cpHDL-AuNRs (R = 250). These results demonstrate that both oleate and cpHDL are present in the organic layer of cpHDL-AuNRs.

The zeta-potential of cpHDL-AuNRs increased linearly with an increasing cpHDL/AuNR weight ratio and reached a plateau of −21 mV at 0.4 (Figure 3a). In accordance with this behavior, the increase in the amount of cpHDL bound to AuNRs was linearly dependent on the cpHDL/AuNR weight ratio and reached a constant value at the same ratio (Figure 3b). Irrespective of the lipid/protein molar ratio (R = 100 or 250), both plots reached a plateau at the same value of 0.4, but the amount of bound protein for R = 100 was about half of that for R = 250 (Figure 3b), consistent with TEM data showing a thinner organic layer for R = 100 than for R = 250 (Figures S3c,d and S8). These results unambiguously show that cpHDL (R = 250) is more advantageous for binding to oleate-AuNRs. This binding was quite stable in PBS, with only 14% of the protein released from the surface during a 4 h incubation at 37 °C (Figure 3c). In the presence of serum, the released amount seemed to be comparable until 4 h (data not shown).

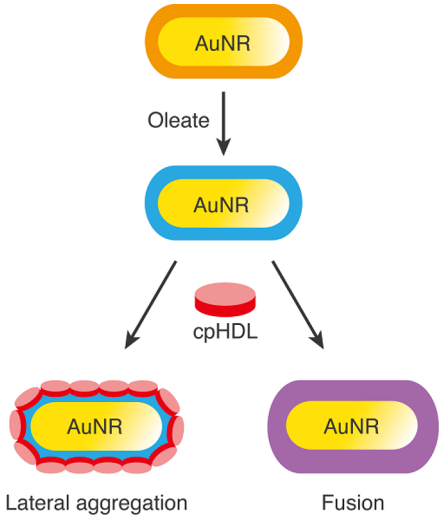

Figure 4. Schematic illustration of surface-engineered AuNRs. For cpHDL binding to oleate-AuNRs, two models are conceivable. In the lateral aggregation model, oleate-AuNRs are coated with a lateral aggregate of cpHDL, whereas fusion (more precisely, intercalation) between the oleate layer and the phospholipid bilayer of cpHDL occurs upon cpHDL binding in the fusion model.

Based on these results and on the average thickness of the organic layer of cpHDL-AuNRs (R = 250) (*ca.* 7.0 nm) and that of the lipid bilayer of cpHDL (5 nm), two models are conceivable for the structure of cpHDL-AuNRs (Figure 4).[30] One structure has a lateral aggregate of cpHDL partially embedded into the oleate layer, while the other involves a fused layer of oleate and cpHDL. We first assessed the possibility of the lateral aggregation model by comparing the amounts of protein per AuNR determined from the SDS-PAGE data in Figure 3b and the amounts derivable from the model (Table S1). The model-based amounts of 60 and 44 apoA-Is per AuNR for cpHDL (R = 100 and 250, respectively) were found to be much smaller than the SDS-PAGE values of 115 and 230 for apoA-Is,

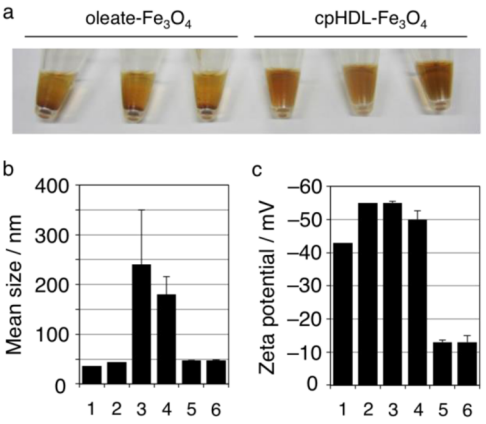

Figure 5. Applicability of our procedure to magnetite nanoparticles (Fe_3O_4). (a) Photograph of aqueous dispersions of oleate-treated (oleate-Fe_3O_4) and oleate/cpHDL-treated magnetite nanoparticles (cpHDL-Fe_3O_4) after 24 h incubation in PBS at 37 °C. Size (b) and zeta-potential data (c) for oleate-Fe_3O_4 and cpHDL-Fe_3O_4; Fe_3O_4 in H_2O (lane 1); oleate-Fe_3O_4 in H_2O (lane 2); oleate-Fe_3O_4 in PBS before (lane 3) and after (lane 4) 24 h incubation at 37 °C; cpHDL-Fe_3O_4 in PBS before (lane 5) and after (lane 6) 24 h incubation at 37 °C. Fe_3O_4, aggregates of 10 nm magnetite nanoparticle, was treated with oleate followed by cpHDL (R = 250) in a similar manner. Whereas oleate-Fe_3O_4 rapidly aggregated in PBS, cpHDL-Fe_3O_4 showed excellent colloidal stability. No change in zeta-potential of cpHDL-Fe_3O_4 during incubation clearly demonstrates that cpHDL is stably bound to Fe_3O_4.

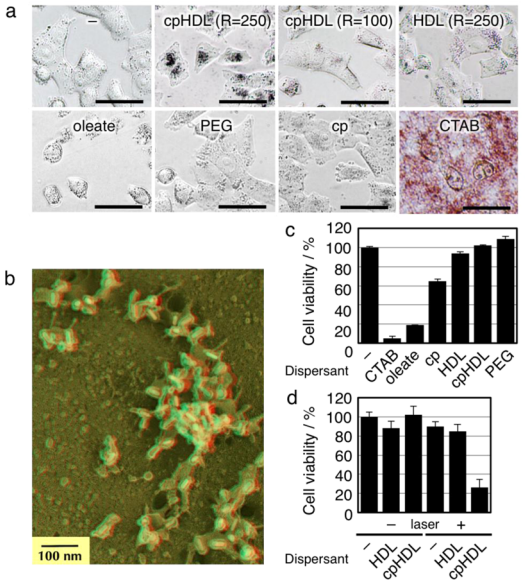

Figure 6. Cell interaction, cytotoxicity, and photothermal effect of cpHDL-AuNRs. (a) Phase contrast images of NCI-H460 cells after 4 h of treatment at 50 μg/mL AuNRs (=630 μM on a Au atom basis). Only the dispersants are indicated in the images. (b) Freeze-fracture TEM image of the outer surface of the plasma membrane after 10 min of treatment with cpHDL-AuNRs (R = 250). (c) Cell viability after 4 h of treatment. Although CTAB was almost entirely removed, oleate-AuNRs showed a significant cytotoxicity, probably due to an adverse effect of oleate being an anionic detergent. (d) Cell viability after treatment followed by laser irradiation (750 nm, 1.5 W, 5 min) in a fresh medium without AuNRs. HDLs used in (b–d) were prepared at R = 250. Scale bar, 50 μm.

respectively. In particular, the similar amounts for the two cpHDLs clearly contradict the data in Figure 3. Thus, simple lateral aggregation of cpHDL may be ruled out as the binding mode of cpHDL to oleate-AuNRs; rather, fusion between the two lipidic dispersants in such a way that the amount of protein on the AuNR surface is increased may occur in our procedure. A possible structure of the protein on the surface in this fusion model is a flexible belt thoroughly wrapping around the surface because apoA-I is believed to flexibly wrap around two entirely different surfaces, spherical lipid emulsions in the mature HDL and the edge of lipid bilayers in the nascent HDL, and to adopt extended α-helical structures in both cases.

It should also be noted that cpHDL binding occurred with 20 nm spherical gold nanoparticles (Figure S9), which were byproducts of AuNR synthesis, and in oleate-coated magnetite nanoparticles (oleate-Fe_3O_4) of *ca.* 40 nm in diameter (Figure 5). Like AuNRs, Fe_3O_4 nanoparticles are stimulus-responsive metal nanoparticles, and they are capable of generating heat upon the application of an external oscillating magnetic field.[31] cpHDL (R = 250)-treated oleate-Fe_3O_4 (cpHDL-Fe_3O_4) was stable during 24 h incubation in PBS at 37 °C, compared with oleate-Fe_3O_4 (Figure 5a,b), and negligible change in the zeta-potential (Figure 5c) indicates a stable binding of cpHDL (R = 250) on the Fe_3O_4 surface as observed for AuNRs (Figure 3c). These results indicate that cpHDL (R = 250) binds to oleate-coated metal nanoparticles regardless of their shape and composition. The apoA-I also binds to metal nanoparticles, but their size is limited to ~5 nm.[32,33] Moreover, the density (3 apoA-Is per 5 nm spherical particle = 0.038 protein/nm^2) was about half of that for cpHDL (R = 250) (230 apoA-Is per AuNR = 0.067 protein/nm^2) (Table S1). Therefore, our approach is suitable for stabilizing mesoscopic metal nanomaterials (5–100 nm) that are larger than the native HDL core, as well as introducing apoA-I proteins at higher density.

Phase contrast images of human cancer cells treated with surface-functionalized AuNRs at 50 μg AuNR/mL (=630 μM on a Au atom basis) for 4 h in the presence of serum are shown in Figure 6a. For cpHDL-AuNRs (R = 250), almost all cell centers were intensely dyed dark purple, showing internalization of the AuNRs. cpHDL-AuNRs (R = 100) exhibited poorer internalization than cpHDL-AuNRs (R = 250), indicating that the degree of internalization of cpHDL-AuNRs is dependent on the amount of protein on the surface. In the early phase (10 min), binding of cpHDL-AuNRs (R = 250) to the plasma membrane was observed and most were individually isolated *via* the organic layer (Figure 6b). Confocal, two-photon luminescence and TEM analyses demonstrated that AuNRs delivered by cpHDL (R = 250) accumulated in endosomes and lysosomes (Figures S10–S12). Inductively coupled plasma (ICP) analysis revealed that 6.38 ± 0.07 pg/cell of cpHDL-AuNRs

(R = 250) and 1.43 ± 0.05 pg/cell of HDL-AuNRs (R = 250) were taken up by the cells. In sharp contrast, the amount for PEG-AuNRs was determined to be 0.074 ± 0.008 pg/cell, showing that these nanoparticles were repelled from the cells.[18,19] This increased internalization of cpHDL-AuNRs (R = 250) did not decrease the cell viability (Figure 6c). Similar behavior of cpHDL-Fe_3O_4 occurred in the same cells (Figure S13).

In hyperthermia (41−45 °C), the treatment temperature and duration are the factors to determine survivability of cells.[34] Under near-infrared laser irradiation for 5 min, cpHDL-AuNRs (R = 250) had stronger photothermal cytotoxicity than HDL-AuNRs (R = 250) (Figure 6d). The cell culture medium temperature increased to 50 °C with cpHDL-AuNRs (R = 250) and 44 °C with HDL-AuNRs (R = 250), both of which were higher than 38 °C for the control. The temperature increase was also dependent on the duration of treatment of the cells with cpHDL-AuNRs (Figure S14). These results clearly show that AuNRs delivered by cpHDL (R = 250) are photothermally active in cells.

CONCLUSIONS

In conclusion, we have described a stepwise procedure for preparation of highly biocompatible and cell-interactive AuNRs using two lipidic dispersants: oleate and cpHDL. The structures of oleate- and cpHDL-AuNRs were thoroughly investigated, and our data indicate fusion of the two lipidic dispersants on the surface of cpHDL-AuNR as a major mechanism of the binding. This procedure was applicable to two other mesoscopic nanoparticles with different shape and composition. Efficient photothermal cancer cell cytotoxicity was achieved through massive internalization of the AuNRs. Thus, utilization of oleate and cpHDL may be a simple and effective method for biomedical applications of mesoscopic metal nanoparticles.

METHODS

Materials. General reagents were purchased from Nacalai tesque (Kyoto, Japan). Gold nanorods (AuNRs) coated with cetyltrimethylammonium bromide (CTAB) were obtained from Dai Nippon Toryo Company, Ltd. (Osaka, Japan). Magnetite nanoparticles (Fe_3O_4), which are secondary nanoparticles of 10 nm magnetite, were purchased from Toda Kogyo Corp. (Hiroshima, Japan). 1-Palmitoyl-2-oleoyl-*sn*-glycero-3-phosphocholine (POPC), sodium cholate, and phenol red-free RPMI 1640 medium were obtained from Wako (Osaka, Japan). Tetramethyl rhodamine isothiocyanate (TMR) and 1,2-dioleoyl-*sn*-glycero-3-phosphoethanolamine-*N*-lissamine rhodamine B sulfonyl (Liss Rhod PE) were purchased from Fluka (St. Gallen, Switzerland) and Avanti Polar Lipid, Inc. (Alabaster, AL, USA), respectively. Transferrin, Alexa Fluor 488 conjugate (Alexa488-Tf), Alexa Fluor 546, cysteine-bearing cell-penetrating peptide (cp, CYGRKKRRQRRR), and fetal bovine serum were obtained from Invitrogen (Carlsbad, CA, USA). PEG-thiol (Sunbright ME-050SH, MW 5000) was obtained from NOF Corporation (Tokyo, Japan). *Escherichia coli* strain BL21 was purchased from Novagen (Madison, WI, USA). The expression vector pCOLD I was obtained from Takara Bio Inc. (Shiga, Japan). Spectra/Por dialysis membranes were purchased from Spectrum Laboratories (Rancho Dominguez, CA, USA). Hoechst 33342 and cell-counting kit-8 were obtained from Dojindo Laboratories (Kumamoto, Japan). NAP-5 columns were purchased from GE Healthcare UK Ltd. (Buckinghamshire, UK). Cell culture dishes were obtained from BD Bioscience (San Jose, CA, USA). Chamber slide II and triple-well glass dishes were purchased from Asahi Glass Co., Ltd. (Tokyo, Japan).

Preparation of cpHDL−metal Nanoparticles. cpHDL was prepared as described elsewhere.[23] Briefly, a cell-penetrating peptide (YGRKKRRQRRR)-fused apoA-I mutant (N-terminal 43 amino acids deleted) was produced as a histidine-tagged protein in an *E. coli* expression system and purified on a Ni Sepharose column (GE Healthcare UK). The lyophilized apoA-I mutant was solubilized in PBS containing 4 M urea and then mixed with POPC (NOF Corporation) in PBS containing 30 mg/mL sodium cholate at a lipid/protein molar ratio of 250 (R = 250).[26,35]

CTAB-AuNRs (Dai Nippon Toryo) were centrifuged at 14 000 rpm for 10 min and redispersed in deionized water. This procedure was repeated twice to remove free CTAB. Then, CTAB-AuNRs were treated with 4 mg/mL sodium oleate at 80 °C for 30 min and passed through a NAP-5 column equilibrated with deionized water. The AuNR eluate was mixed with cpHDL at a protein/AuNR weight ratio of 0.4 at 50 °C for 1 h. cpHDL-AuNRs were centrifuged and redispersed in PBS to remove unbound cpHDL. For Fe_3O_4 (Toda Kogyo Corp.), the same procedure was applied, except for use of a protein/Fe_3O_4 weight ratio of 0.8.

Physicochemical Analyses of AuNRs, cpHDL, and Their Complexes. UV−vis−NIR spectra of AuNRs were measured using a Beckman Coulter DU800 spectrophotometer. The hydrodynamic diameter of cpHDL in PBS was determined with a Nanotrac UPA-UT151 (Nikkiso Co., Ltd., Tokyo, Japan). The zeta-potential of AuNRs in 50 mM Tris-HCl (pH 7) was determined with a Zetasizer Nano Z (Malvern Instruments, Malvern, UK). XPS data were acquired using an ULVAC-PHI 5500MT system equipped with a Mg KR X-ray source (1253.6 eV) and a hemispherical energy analyzer. The signals were fitted by Gaussian functions using the program OriginPro 8.6. ^{1}H NMR spectra were measured using a JEOL JNM-EX400 NMR spectrometer in D_2O. FTIR spectra were obtained using a JASCO FT/IR-470 plus spectrometer with a KBr pellet. SDS-PAGE was performed for the apoA-I mutant liberated from AuNRs, and the protein band stained with CBB was densitometrically analyzed using a ChemiDoc XRS Plus system (Bio-Rad, Hercules, CA, USA). For SDS-PAGE of the apoA-I mutant in Figure 3c, cpHDL-AuNRs (R = 250) were prepared with cpHDL (R = 250) labeled with Alexa Fluor 546 on the protein, and the fluorescence intensity of the protein band was measured using the instrument above. In the presence of serum, proteins that bound rapidly to AuNRs and had similar molecular weight to the TAT peptide-fused apoA-I slightly enhanced the fluorescent intensity, which precluded a rigorous evaluation (data not shown). Analysis was performed in duplicate (n = 2).

Cell Culture. Human non-small cell lung cancer NCI-H460 cells were maintained in phenol red-free RPMI 1640 supplemented with 10% FBS, 100 U/mL penicillin, and 100 μg/mL streptomycin. NCI-H460 cells were cultured in 5% CO_2 and 95% air. Cells were passaged every 2−3 days. Phase contrast images of the cells were observed using an Olympus IX71 inverted microscope (Tokyo, Japan).

Transmission Electron Microscopy (TEM) Measurement. The mica flake EM technique was utilized for fine structural analysis of cpHDL-AuNRs. Two drops of a suspension of finely ground muscovite mica flakes were added to 500 μL of a cpHDL-AuNR suspension at 10−100 μg/mL, and cpHDL-AuNRs were allowed to gently adsorb to mica for ~30 s at room temperature. The rapidly frozen slurry of mica flakes was then fractured in a JEOL EM-1950 JFDII freezing unit and immediately deep-etched for 2 min at −104 °C. It was rotary-shadowed with platinum at an

angle of 11° from the surface and with carbon from the top. The replica was separated from the mica, cleaned with hydrofluoric acid, and picked up on Formvar-coated 200 mesh EM grids (copper, hexagonal, thin bar grid; GuilderGrids Co., UK). The replica was observed in a JEOL JEM1400 at 120 kV. The thickness of the organic layer of AuNRs was determined with consideration of the thickness of the platinum layer (2 nm). For Fe_3O_4, this mica flake EM measurement was precluded by dissolution of Fe_3O_4 during hydrofluoric acid treatment.

NCI-H460 cells were seeded at 1.0×10^5 cells/mL and cultured for 1 day on small sapphire glass disks (3 mm in diameter) coated with carbon. Cells were treated with 50 μg/mL cpHDL-AuNRs (R = 250) (AuNR basis) for 0.5−4 h and rapidly frozen. The freeze substitution was carried out in cold 1% OsO_4 in acetone for 50 h at −90 °C, 3 h at −40 °C, and 2 h at 0 °C. Then the specimen was washed with pure dry acetone at room temperature and embedded in Epon 812 (TAAB, UK). After polymerization at 65 °C for a few days, ultrathin sections (~60 nm) made with an Ultramicrotome (Leica FC6, Vienna, AU) were mounted in EM grids, stained with lead citrate, and observed by conventional TEM (JEOL JEM1400, Japan). The freeze-dry technique for observation of plasma membrane-bound AuNRs has been described elsewhere.[36] EM anaglyphs were generated from tilted images at ±10°. Use red and green glasses for the 3D structure (with red to the left).

Two-Photon Luminescence Microscopy. After treatment with cpHDL-AuNRs (R = 250) for 4 h, cell nuclei were stained with Hoechst 33342. Two-photon luminescence images were obtained using a Carl Zeiss LSM 780 NLO confocal system equipped with a Chameleon femtosecond pulsed laser. AuNRs were excited at 786 nm.

Confocal Microscopy. cpHDL (R = 250) was labeled on the protein moiety with tetramethyl rhodamine isothiocyanate (TMR), as described previously with a minor modification.[37] Briefly, cpHDL (R = 250) was mixed with TMR on ice at a cpHDL/TMR weight ratio of 100 in 0.1 M $NaHCO_3$ (pH 8). After mild rotation at 4 °C for 4 h, unbound TMR was removed with a NAP-5 gel filtration column (GE Healthcare) equilibrated with PBS, followed by dialysis against PBS at 4 °C for a few days. Then, TMR-labeled cpHDL (R = 250) was mixed with oleate-AuNRs. For Liss Rhod PE labeling of Fe_3O_4, cpHDL and HDL were prepared using POPC containing 1% Liss Rhod PE, and then the HDLs were mixed with oleate-Fe_3O_4. NCI-H460 cells were treated with TMR-labeled cpHDL-AuNRs (R = 250) for 4 h. During the last 30 min, the cells were co-treated with Alexa488-Tf. Confocal images were acquired using an Olympus confocal laser scanning microscope FV10i-LIV.

ICP Analysis of AuNRs in Cells. After treatment with cpHDL-AuNRs (R = 250) or HDL-AuNRs (R = 250), cells were washed by PBS twice, scraped, and centrifuged at 1000 rpm for 5 min. The cell pellets were incubated in aqua regia for 4 h, and the reaction solution was evaporated. The residue was dissolved in 1 mM HCl, and Au ions were quantified using a Shimadzu plasma atomic emission spectrometer ICPE-9000 (Kyoto, Japan).

Cell Viability Assay. NCI-H460 cells were seeded at 1×10^5 cells/mL and cultured for 1 day. After treatment with AuNRs (50 μg AuNR/mL) for 4 h in the cell culture medium, the cells were washed with the medium. For the photothermal study, the cells were further irradiated at 750 nm laser at 1.5 W (Chameleon-RF, Coherent) for 5 min. After irradiation, the temperature of the medium was measured with a fiber optic temperature sensor ReflexTM (Neoptix). Cell viabilities were evaluated using a cell-counting kit-8 and a SpectraMax M2 microplate reader (Molecular Devices) and normalized ($OD_{450}-OD_{620}$) with respect to untreated cells. Assays were performed in triplicate.

Preparation of PEG-AuNRs and cp-AuNRs. PEG- and cp-AuNRs were prepared as described elsewhere.[11,38] Briefly, CTAB-AuNRs were first centrifuged at 15 000g for 10 min and redispersed in deionized water to remove free CTAB. Thiol-PEG (MW 5000, NOF Corporation) (5 molar equiv) was mixed with the AuNRs, and the mixture was stirred for 24 h at room temperature in the dark. PEG-AuNRs were purified by dialysis (MWCO 50 000) against 3 L of deionized water for 3 days. The cysteine-bearing cell-penetrating peptide (1 mM) was mixed with the AuNRs (Abs_{max} = 1), and the mixture was incubated at room temperature for 3 days in the dark. cp-AuNRs were purified by centrifugation (15 000g, 10 min) and redispersed in deionized water. Successful conjugation was indicated by the zeta-potential (−3.6 ± 0.4 mV for PEG-AuNRs and 2.3 ± 1.9 mV for cp-AuNRs).

Conflict of Interest: The authors declare no competing financial interest.

Acknowledgment. This work was supported by the World Premier International Research Center Initiative (WPI), MEXT, Japan, and by PRESTO, JST (T.M.), a Grant-in-Aid for Scientific Research (B) (T.M.), a Health Labor Sciences Research Grant (nano-001 to N.M.), and Innovative Areas, MEXT (N.M.).

Supporting Information Available: Dynamic light scattering analysis of cpHDLs (Figure S1); UV−vis−NIR absorption spectra of AuNRs used in this study (Figure S2); histograms of the thickness of the organic layer in TEM images in Figure 1 (Figure S3); ^{1}H NMR spectra of CTAB- and oleate-AuNRs (Figure S4); FTIR spectra of CTAB-, oleate-, and cpHDL-AuNRs (Figure S5); stability of cpHDL-AuNRs (R = 250) (Figure S6); UV−vis−NIR absorption spectra and cytotoxicity of CTAB-AuNRs before and after mixing with cpHDL (R = 250) (Figure S7); mica flake TEM images of cpHDL-AuNRs (R = 100) (Figure S8); mica flake TEM image of a cpHDL (R = 250)-bound spherical gold nanoparticle (Figure S9); Confocal analysis of fluorescently labeled cpHDL-AuNRs (R = 250) (Figure S10); two-photon luminescence microscopy analysis of cpHDL-AuNRs (R = 250) (Figure S11); TEM analysis of cpHDL-AuNRs (R = 250) bound to and internalized by cells (Figure S12); cell interaction and cytotoxicity of cpHDL-Fe_3O_4 (Figure S13); treatment−duration dependency of photothermal heating (Figure S14); schematic illustration of AuNRs used in Table S1 (Figure S15); amount of protein per AuNRs determined by SDS-PAGE analysis in Figure 3b and calculated based on the lateral aggregation model (Table S1). This material is available free of charge *via* the Internet at http://pubs.acs.org.

REFERENCES AND NOTES

1. Melancon, M. P.; Zhou, M.; Li, C. Cancer Theranostics with Near-Infrared Light-Activatable Multimodal Nanoparticles. *Acc. Chem. Res.* **2011**, *44*, 947–956.
2. Jain, K. K. Advances in the Field of Nanooncology. *BMC Med.* **2010**, *8*, 83.
3. Yu, Y.-Y.; Chang, S.-S.; Lee, C.-L.; Wang, C. R. C. Gold Nanorods: Electrochemical Synthesis and Optical Properties. *J. Phys. Chem. B* **1997**, *101*, 6661–6664.
4. Mohamed, M. D.; Ismail, K. Z.; Link, S.; El-Sayed, M. A. Thermal Reshaping of Gold Nanorods in Micelles. *J. Phys. Chem. B* **1998**, *102*, 9370–9374.
5. Link, S.; Mohamed, M. D.; El-Sayed, M. A. Simulation of the Optical Absorption Spectra of Gold Nanords as a Function of Their Aspect Ratio and the Effect of the Medium Dielectric Constant. *J. Phys. Chem. B* **1999**, *103*, 3073–3077.
6. Jain, P. K.; Lee, K. S.; El-Sayed, I. H.; El-Sayed, M. A. Calculated Absorption and Scattering Properties of Gold Nanoparticles of Different Size, Shape, and Composition: Applications in Biological Imaging and Biomedicine. *J. Phys. Chem. B* **2006**, *110*, 7238–7248.
7. Bouhelier, A.; Bachelot, R.; Lerondel, G.; Kostcheev, S.; Royer, P.; Wiederrecht, G. P. Surface Plasmon Characteristics of Tunable Photoluminescence in Single Gold Nanorods. *Phys. Rev. Lett.* **2005**, *95*, 267405.
8. Huang, X.; Jain, P. K.; El-Sayed, I. H.; El-Sayed, M. A. Gold Nanoparticles: Interesting Optical Properties and Recent Applications in Cancer Diagnostics and Therapy. *Nanomedicine (London, U. K.)* **2007**, *2*, 681–693.
9. Tong, L.; Wei, Q.; Wei, A.; Cheng, J.-X. Gold Nanorods as Contrast Agents for Biological Imaging: Optical Properties, Surface Conjugation and Photothermal Effects. *Photochem. Photobiol.* **2009**, *85*, 21–32.
10. Alkilany, A. M.; Naggria, P. K.; Hexel, C. R.; Shaw, T. S.; Murphy, C. J.; Wyatt, M. D. Cellular Uptake and Cytotoxicity of Gold Nanorods: Molecular Origin of Cytotoxicity and Surface Effects. *Small* **2009**, *5*, 701–708.

11. Niidome, T.; Yamagata, M.; Okamoto, Y.; Akiyama, Y.; Takahashi, H.; Kawano, T.; Katayama, Y.; Niidome, Y. PEG-Modified Gold Nanorods with a Stealth Character for *In Vivo* Applications. *J. Controlled Release* **2006**, *114*, 343–347.
12. Prencipe, G.; Tabakman, S. M.; Welsher, K.; Liu, Z.; Goodwin, A. P.; Zhang, L.; Henry, J.; Dai, H. PEG Branched Polymer for Functionalization of Nanomaterials with Ultralong Blood Circulation. *J. Am. Chem. Soc.* **2009**, *131*, 4783–4787.
13. Von Maltzahn, G.; Park, J.-H.; Agrawal, A.; Bandaru, N. K.; Das, S. K.; Sailor, M. J.; Bhatia, S. N. Computationally Guided Photothermal Tumor Therapy Using Long-Circulating Gold Nanorod Antennas. *Cancer Res.* **2009**, *69*, 3892–3900.
14. Bonoiu, A. C.; Bergey, E. J.; Ding, H.; Hu, R.; Kumar, R.; Yong, K.-T.; Prasad, P. N.; Mahajan, S.; Picchione, K. E.; Bhattacharjee, A.; Ignatowski, T. A. Gold Nanorod-siRNA Induces Efficient *In Vivo* Gene Silencing in the Rat Hippocampus. *Nanomedicine (London, U. K.)* **2011**, *6*, 617–630.
15. Chakravarthy, K. V.; Bonoiu, A. C.; Davis, W. G.; Ranjan, P.; Ding, H.; Hu, R.; Bowzard, J. B.; Bergey, E. J.; Katz, J. M.; Knight, P. R.; Sambhara, S.; Prasad, P. N. Gold Nanorod Delivery of an ssRNA Immune Activator Inhibits Pandemic H1N1 Influenza Viral Replication. *Proc. Natl. Acad. Sci. U.S.A.* **2010**, *107*, 10172–10177.
16. Lee, S. E.; Liu, G. L.; Kim, F.; Lee, L. P. Remote Optical Switch for Localized and Selective Control of Gene Interference. *Nano Lett.* **2009**, *9*, 562–570.
17. Huang, X.; El-Sayed, I. H.; Qian, W.; El-Sayed, M. A. Cancer Cell Imaging and Photothermal Therapy in the Near-Infrared Region by Using Gold Nanorods. *J. Am. Chem. Soc.* **2006**, *128*, 2115–2120.
18. Alkilany, A.; Shatanawi, A.; Kurtz, T.; Caldwell, R. B.; Caldwell, R. W. Toxicity and Cellular Uptake of Gold Nanorods in Vascular Endothelium and Smooth Muscles of Isolated Rat Blood Vessel: Importance of Surface Modification. *Small* **2012**, *8*, 1270–1278.
19. Huff, T. B.; Hansen, M. N.; Zhao, Y.; Cheng, J.-X.; Wei, A. Controlling the Cellular Uptake of Gold Nanorods. *Langmuir* **2007**, *23*, 1596–1599.
20. Stefanick, J. F.; Ashley, J. D.; Kiziltepe, T.; Bilgicer, B. A Systemic Analysis of Peptide Linker Length and Liposomal Polyethylene Glycol Coating on Cellular Uptake of Peptide-Targeted Liposomes. *ACS Nano* **2013**, *7*, 2935–2947.
21. Enselme, J. *Unsaturated Fatty Acids in Atherosclerosis*; Pergamon Press: London, 1969.
22. Lund-Katz, S.; Phillips, M. C. High Density Lipoprotein Structure—Function and Role in Reverse Cholesterol Transport. In *Cholesterol Binding and Cholesterol Transport Proteins: Structure and Function in Health and Disease*, Harris, J. R., Ed.; Springer-Verlag: Heidelberg, 2010; pp 183—227.
23. Murakami, T.; Wijagkanalan, W.; Hashida, M.; Tsuchida, K. Intracellular Drug Delivery by Genetically Engineered High Density Lipoprotein Nanoparticles. *Nanomedicine (London, U. K.)* **2010**, *5*, 867–879.
24. Chauhan, A.; Tikoo, A.; Kapur, A. K.; Singh, M. The Taming of the Cell Penetrating Domain of the HIV Tat: Myths and Realities. *J. Controlled Release* **2007**, *117*, 148–162.
25. Palm-Apergi, C.; Lönn, P.; Dowdy, S. F. Do Cell-Penetrating Peptides Acutually "Penetrate" Cellular Membranes? *Mol. Ther.* **2012**, *20*, 695–697.
26. Murakami, T.; Tsuchida, K.; Hashida, M.; Imahori, H. Size Control of Lipid-Based Drug Carriers by Drug Loading. *Mol. BioSyst.* **2010**, *6*, 789–791.
27. Nikoobakht, B.; El-Sayed, M. A. Evidence for Bilayer Assembly of Cationic Surfactants on the Surface of Gold Nanorods. *Langmuir* **2001**, *17*, 6368–6374.
28. Hubert, F.; Testard, F.; Spalla, O. Cetyltrimethylammonium Bromide Silver Bromide Complex as the Capping Agent of Gold Nanorods. *Langmuir* **2008**, *24*, 9219–9222.
29. Murphy, C. J.; Gole, A. M.; Hunyadi, S. E.; Stone, J. W.; Sisco, P. N.; Alkilany, A.; Kinard, B. E.; Hankins, P. Chemical Sensing and Imaging with Metallic Nanorods. *Chem. Commun.* **2008**, 544–557.
30. As the third model, protein aggregation model, in which aggregation of the protein in cpHDL is induced in some way, is also conceivable because it potentially allows high-density binding of the protein. However, this model is quite unlikely to be a major mechanism of the binding, based on the fact that the colloidal stability of cpHDL-AuNRs (R = 250) was quite high (Figures S2a and S6a,c), and that HDL aggregates had a propensity to precipitate.[26]
31. Chandra, S.; Barick, K. C.; Bahadur, D. Oxide and Hybrid Nanostructures for Therapeutic Applications. *Adv. Drug Delivery Rev.* **2011**, *63*, 1267–1281.
32. Cormode, D. P.; Skajaa, T.; van Schooneveld, M. M.; Koole, R.; Jarzyna, P.; Lobatto, M. E.; Calcagno, C.; Barazza, A.; Gordon, R. E.; Zanzonico, P.; Fisher, E. A.; Fayad, Z. A.; Mulder, W. J. M. Nanocrystal Core High-Density Lipoproteins: A Multimodality Contrast Agent Platform. *Nano Lett.* **2008**, *8*, 3715–3723.
33. Thaxton, C. S.; Daniel, W. L.; Giljohann, D. A.; Thomas, A. D.; Mirkin, C. A. Templated Spherical High Density Lipoprotein Nanoparticles. *J. Am. Chem. Soc.* **2009**, *131*, 1384–1385.
34. Gerweck, L. E. Hyperthermia in Cancer Therapy: The Biological Basis and Unresolved Questions. *Cancer Res.* **1985**, *45*, 3408–3414.
35. Matz, C. E.; Jonas, A. Micellar Complexes of Human Apolipoprotein A-I with Phosphatidylcholines and Cholesterol Prepared from Cholate-Lipid Dispersions. *J. Biol. Chem.* **1982**, *257*, 4535–4540.
36. Numata, T.; Murakami, T.; Kawashima, F.; Morone, N.; Heuser, J. E.; Takano, Y.; Ohkubo, K.; Fukuzumi, S.; Mori, Y.; Imahori, H. Utilization of Photoinduced Charge-Separated State of Donor-Acceptor-Linked Molecules for Regulation of Cell Membrane Potential and Ion Transport. *J. Am. Chem. Soc.* **2012**, *134*, 6092–6095.
37. Takata, K.; Horiuchi, S.; Torab, A.; Rahim, M. A.; Morino, Y. Receptor-Mediated Internalization of High Density Lipoprotein by Rat Sinusoidal Liver Cells: Identification of a Nonlysosomal Endocytic Pathway by Fluorescence-Labeled Ligand. *J. Lipid Res.* **1988**, *29*, 1117–1126.
38. de la Fuente, J. M.; Berry, C. C. Tat Peptide as an Efficient Molecule To Translocate Gold Nanoparticles into the Cell Nucleus. *Bioconjugate Chem.* **2005**, *16*, 1176–80.